

Extragalactic cosmic rays and their signatures

V. Berezhinsky

INFN, National Gran Sasso Laboratory, I-67010, Assergi (AQ) Italy

Abstract

The signatures of UHE proton propagation through CMB radiation are pair-production dip and GZK cutoff. The visible manifestations of these two spectral features are ankle, which is intrinsic part of the dip, beginning of GZK cutoff in the differential spectrum and $E_{1/2}$ in integral spectrum. Observed practically in all experiments since 1963, the ankle is usually interpreted as a feature caused by transition from galactic to extragalactic cosmic rays. Using the mass composition measured by HiRes, Telescope Array and Auger detectors at energy (1 - 3) EeV, calculated anisotropy of galactic cosmic rays at these energies, and the elongation curves we strongly argue against the interpretation of the ankle given above. The transition must occur at lower energy, most probably at the second knee as the dip model predicts. The other prediction of the dip model, the shape of the dip, is well confirmed by HiRes, Telescope Array (TA), AGASA and Yakutsk detectors, and, after recalibration of energies, by Auger detector. Predicted beginning of GZK cutoff and $E_{1/2}$ agree well with HiRes and TA data. However, directly measured mass composition remains a puzzle. While HiRes and TA detectors observe the proton-dominated mass composition, as required by the dip model, the data of Auger detector strongly evidence for nuclei mass composition becoming progressively heavier at energy higher than 4 EeV and reaching Iron at energy about 35 EeV. The Auger-based scenario is consistent with another interpretation of the ankle at energy $E_a \approx 4$ EeV as transition from extragalactic protons to extragalactic nuclei. The heavy - nuclei dominance at higher energies may be provided by low-energy of acceleration for protons $E_p^{\max} \sim 4$ EeV and rigidity-dependent $E_A^{\max} = ZE_p^{\max}$ for nuclei. The highest energy suppression may be explained as nuclei-photodisintegration cutoff.

Keywords: Cosmic rays, 96.50.S, energy spectra, 96.50.sb, galactic and extragalactic, 98.70.Sa

1. Historical review: galactic or extragalactic origin?

Do observed cosmic rays (CR) have galactic or extragalactic origin? Since late 1950s this question divided theorists in two groups. V.L. Ginzburg [1] and S.I. Syrovatsky [2], defended the Galactic origin, while F. Hoyle [3], G.R. Burbidge [4, 5] and their collaborators suggested the extragalactic origin. In 1963 in book [6] Ginzburg and Syrovatsky presented the strong arguments in favour of galactic origin, but hot discussions between these two groups continued at all International Cosmic Ray Conferences (ICRC) until late 1980s.

The main issues of extragalactic origin have been acceleration, diffusive propagation of extragalactic particles and magnetic fields in galaxies and clusters. The main point of extragalactic models was proposal of Active Galactic Nuclei (AGN) as the sources, and explanation of observed isotropy of cosmic rays. Much attention was given to acceleration of protons to highest energies above 10^{19} eV, impossible in Galactic model. An upper limit to the maximum energy of acceleration was found in [5] from condition of equality of the Larmor radius and dimension of the accelerating site, which later was used in the famous “Hillas plot” [7]. As a plausible model in [4] was proposed the the Local Supercluster with AGN observed there.

V.L. Ginzburg suggested the rigorous test for extragalactic origin, predicting the lower-limit for gamma-ray flux from Small Magellanic Cloud (SMC). The gas density in this source is fairly well known, while the CR flux in extragalactic model is that measured in Milky Way (MW). Therefore, the produced gamma-ray flux at energies $E_\gamma \gtrsim 100$ MeV is well predicted. The calculated gamma-ray flux from $pp \rightarrow \pi^0$ production gives the lower limit, because part of the detected flux can be produced by electrons and by the point-like sources. In 1993 EGRET [8] put the upper limit to gamma-ray flux from SMC well below the Ginzburg lower limit, which means that extragalactic CR flux is lower than that observed in MW. In 2008 Fermi/LAT [9] measured gamma-ray flux from SMC with a high accuracy, reliably excluding extragalactic origin of the bulk of CRs observed in our galaxy. The exclusion obtained by EGRET and FERMI/LAT is not valid for very high CR energies where transition to extragalactic CRs may be expected.

The Standard Model (SM) for Galactic Cosmic Rays was first put forward by Ginzburg and Syrovatskii [6] in 1963 and in the main features it was accomplished in 1977 - 1978 by discovery of diffusive shock acceleration [11]. The SM is based on (i) supernova remnants as sources, (ii) SNR shock

acceleration, and (iii) diffusive propagation of CR in the Galactic magnetic fields.

The book [6] was not a review. It described an original and detailed construction of Galactic model of cosmic rays and their propagation in magnetic fields. The book included the theoretical issues of synchrotron radiation relative to astrophysics, and diffusion equations for propagation of particles with their analytic solutions. In particular, the remarkable Syrovatsky analytic solution of diffusion equation for point-like sources [10] was included there. However, most important results were obtained phenomenologically. The authors put forward the disc-halo model and estimated the magnetic fields B there, suggesting equipartition relation $\omega_{\text{cr}} \sim B^2/2\pi \sim \rho u^2/2$, where the first term is energy density of cosmic rays and the last one is turbulent energy density of plasma. Magnetic field in the disc was estimated as $B_d \sim 3 \times 10^{-6}$ G. Two versions of halo were suggested and analysed: the spherical one with $R_h \sim 10 - 15$ kpc and with flattening halo with $h \sim 3$ kpc. The set of diffusion equations for protons and nuclei was solved analytically and, using the data on anisotropy and mass composition, diffusion coefficient for disc was estimated as $D \sim 1 \times 10^{29}$ cm²/s, close to presently known value. The authors recognised the problem of Li , Be , B as the secondary nuclei and using the solutions of diffusion equations for many nuclei and galactic models, determined the thickness traversed by cosmic rays as $x \sim 10$ g/cm², also close to the present value. Finally, the authors estimated the galaxy luminosity in cosmic rays L_{cr} using two formulae which at present can be unified as

$$L_{\text{cr}} \sim c\omega_{\text{cr}}M_g/x \quad (1)$$

where M_g is the mass of galactic gas. Eq. (1) gives $L_{\text{cr}} \sim 2 \times 10^{40}$ erg/s in a good agreement with energy release of SN in our Galaxy.

The most interesting and dramatic story in development of SM is connected with acceleration.

In 1977-1978 four works on acceleration at shocks [11] appeared almost simultaneously. The particles are accelerated due to multiple reflections from the shock front and may acquire maximum energy high enough for galactic cosmic rays. In 1983 Laggage and Cesarsky [12] demonstrated that the time of acceleration cycle increases during process of acceleration and E_{max} remains below the observed knee, which is galactic feature. It was really a dramatic moment, when most reliable and beautiful acceleration mechanism seems to be not viable. Revival came back not very soon: in 2001 Bell

and Lucek [13] convincingly confirmed the early proposal of Bell [11] about strong amplification of magnetic field upstream by cosmic rays themselves due to streaming instability. A highly turbulent field with strength up to $B \sim 10^{-4}$ G is produced and increases maximum energy up to needed value $E_{\max} \sim 4Z$ PeV.

2. Spectral features and signatures.

The observed energy spectrum of Cosmic Rays (CR) has approximately a power-law behavior for 11 orders of magnitude in energy with several features that can be linked with particles propagation and acceleration.

The most prominent spectral feature is the *knee* in all-particle spectrum at energy 3-4 PeV, discovered first at the MSU (Moscow State University) array in 1958 [14]. At the knee the spectrum $E^{-\gamma}$ steepens from $\gamma \approx 2.7$ to $\gamma \approx 3.1$. This knee is provided by the light elements, protons and Helium, and is explained in the framework of the Standard Model (SM) for Galactic Cosmic Rays (GCR) by the maximum energy E_{\max} of acceleration in the Galactic Sources (Supernovae Remnants, SNR). In the case of the rigidity-dependent acceleration $E_{\max} \propto Z$, where Z is charge number of a nuclei, the maximum acceleration energy is reached by Iron nuclei, and thus the Iron knee is predicted to be located at energy by factor 26 times higher than for proton knee, i.e. at energy $E_{\max}^{\text{Fe}} \sim (80 - 100)$ PeV. Recently, the Iron knee was found indeed at energy 80 PeV in KASCADE-Grande experiment [15] in a good agreement with rigidity-acceleration prediction.

Above the knee, at energy $E_{\text{skn}} \approx (0.4 - 0.7)$ EeV, there is a faint feature in the spectrum [16] called the *second knee*. It is seen in many experiments (for a review see [17]). This feature is often interpreted as a place of transition from galactic to extragalactic CRs. However, for the last forty years the standard place for transition from galactic to extragalactic CRs is considered at *ankle*, a very prominent spectral feature, observed first in 1960s by Volcano Ranch detector at energy $E_a^{\text{obs}} \sim 10$ EeV, and it was immediately interpreted by J. Linsley [18] as transition between these two components of CRs. This interpretation was further confirmed by detection a particle with energy about 100 EeV [19]. The ankle as presented by J. Linsley in 1973 [20] is shown in Fig. 1 according to data of Volcano-Ranch and Haverah-Park. (Fig. 1 is taken from paper by T.K. Gaisser [21]). At present beginning of ankle is found at $E_a^{\text{obs}} \approx 4.5 \pm 0.5$ EeV according to HiRes observations [22],

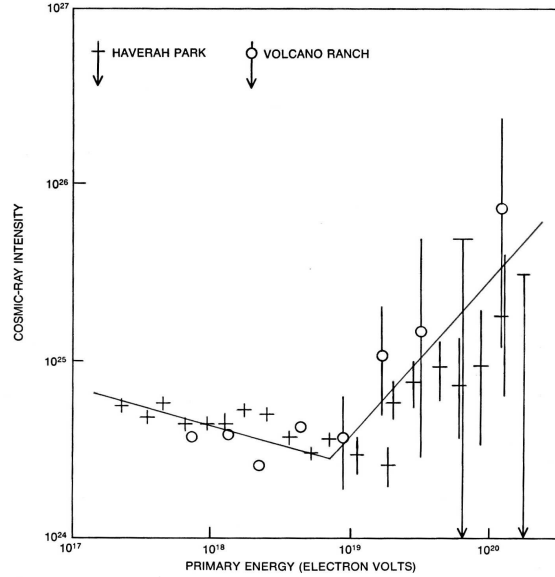


Figure 1: The ankle as presented by J. Linsley in review [20] and taken from paper by T.K. Gaisser [21].

at (4.9 ± 0.3) EeV in Telescope Array (TA) [23], and at (4.2 ± 0.1) EeV in Auger (PAO) [24, 25].

What makes us think that CR at highest energies are extragalactic and that transition occurs at ankle?

If CRs at highest energies are galactic heavy nuclei up to Iron, anisotropy can be not easily observable. However, SNRs as the sources cannot provide particles with energies as high as 100 EeV, and for all-galactic-CR model one needs additional class of sources which are able to accelerate particles to much higher energies than SNR. These sources can be hypernovae explosions (GRBs) which occur very rarely, e.g. one per million years in our galaxy. Such a model was developed in [26]. More recently another galactic model [27] also with GRBs as the sources was studied, with protons and Iron nuclei as accelerated particles and assuming diffusion of Iron nuclei in the galactic magnetic fields. The calculated energy spectrum explains well the observed PAO spectrum.

To prove that observed particles at highest energies are extragalactic, one must know their signatures, and these signatures have been found theoretic-

cally in famous works by K. Greisen [28] and G.T. Zatsepin and V.A. Kuzmin [29], who predicted that extragalactic protons propagating through CMB radiation obtain the specific steepening of energy spectrum, called Greisen-Zatsepin-Kuzmin (GZK) cutoff.

The highest energy feature, the steepening ('cutoff') of the spectrum is found indeed in all three largest detectors, HiRes [30], Telescope Array (TA) [31] and PAO [32], though the nature of this cutoff is still questionable.

The spectrum steepening is quite different for protons and nuclei as primaries. The energy losses and lifetimes of these particles interacting with CMB and EBL (Extragalactic Background Light) photons are shown in Fig.2.

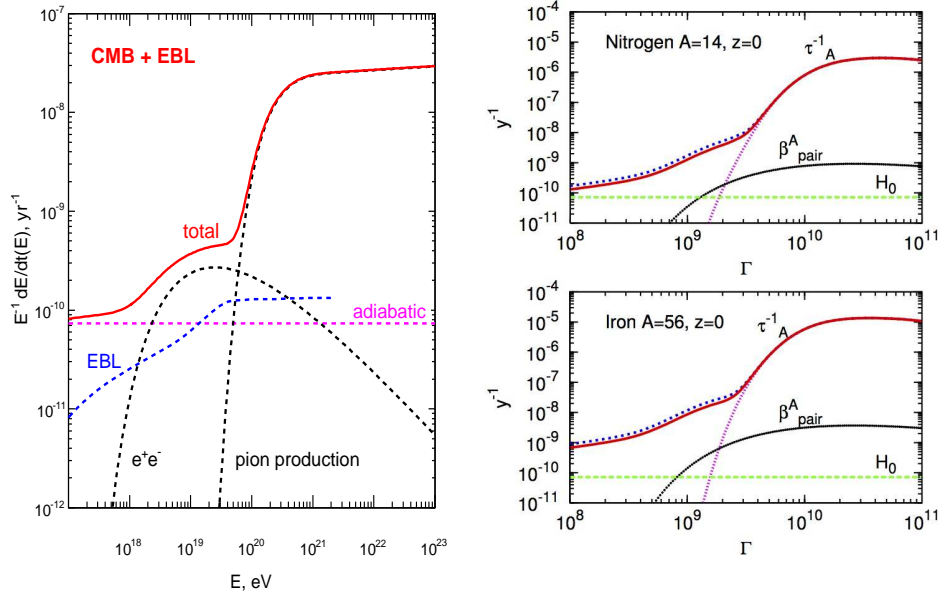


Figure 2: Energy losses of protons (left panel) on CMB and EBL. One can see that energy losses on EBL can be neglected. There are two characteristic energies: $E_{eq1} = 2.4$ EeV (intersection of pair-production e^+e^- and adiabatic curves) and $E_{eq2} = 61$ EeV (intersection of pair- and pion- production curves). It is clear that beginning of the GZK cutoff must be about (but below) E_{q2} . In the right panel the inverse lifetimes of two nuclei, Nitrogen and Iron, are shown as function of Lorentz factor Γ from [33, 34]. The dotted curves show contribution of EBL. The small-dots lines show the case of CMB only, which corresponds to steepening at intersection of pair-production curve (line β_{pair}^A) with adiabatic curve H_0 . Presence of EBL strongly modifies this picture. See text for more details.

The GZK cutoff is caused by photopion production on CMB photons:

$$p + \gamma_{\text{cmb}} \rightarrow N + \pi. \quad (2)$$

The energy $E_{\text{eq2}} \approx 60$ EeV (see Fig. 2) describes this steepening as interaction signature. In realistic calculations beginning of the GZK cutoff is lower, because at larger z the intersection point $E_{\text{eq2}}(z)$ is shifted by factor $(1+z)$ to lower energies. The spectrum must show steepening at lower energy $E_{\text{GZK}} \approx 50$ EeV, though this is (weakly) model-dependent quantity. However, the PAO data for beginning of steepening $\log E_{\text{GZK}} = 19.41 \pm 0.02$, with E in eV, (or $E_{\text{GZK}} = 25.7 \pm 1.2$ EeV) given in Table 1 of [35] is below all known theoretical predictions, even after taking into account a possible 22% energy shift due to systematic energy errors.

On the other hand HiRes [30] and TA [31] data agree well with predicted beginning of the GZK cutoff and its energy shape. This contradiction reflects the different mass composition found in these experiments. In the discussed energy region the mass composition of PAO is presented by heavy nuclei and the observed spectrum cutoff might be explained as *nuclei-photodisintegration* cutoff (see nuclei lifetimes in the right panel of Fig.2). In this panel the continuous pair-production energy losses β_{pair}^A and adiabatic energy losses (curve H_0) are shown together with lifetime of photodisintegration on CMB (small-dots lines) and EBL (dotted curves). The calculated lifetimes (from recent papers [33] and [34]) correspond to emission of one and more nucleons. The Lorentz-factor Γ as energy variable in Fig. 2 is chosen because it is practically not changed in the process of photodisintegration. It changes mainly due to pair-production on CMB at large Γ and adiabatic energy-loss at lower Γ . If one is interested in any nucleus A produced at propagation of accelerated nucleus A_0 , its energy $E = Am_N\Gamma$ changes in all three processes described above (for more details see [33, 34] and review [36]). If to include in consideration only CMB, then $E^{-1}dE/dt$ strongly increases after crossing the adiabatic energy loss by pair-production curve. Qualitatively one can see it in the right panels of Fig. 2 in case of small-dots curves. Then situation reminds the GZK cutoff and photodisintegration spectrum-steepening is only a little lower than in case of GZK. This was first demonstrated in works [37, 38] in 1971 and 1975, respectively. Presence of EBL radically changes this picture, because nuclei are photodisintegrated faster than they lose kinetic energy. The dependence of photodisintegration time on Lorentz-factor becomes smoother (see the dotted curves in Fig. 2). A possible efficient pho-

photodisintegration of UHE nuclei on extragalactic light was first demonstrated by N.M. Gerasimova and I.L. Rozental in 1961 [39].

If one considers the energy spectra with fixed A , e.g. the primary nuclei only, the steepening of the spectrum is produced by increasing of τ_A^{-1} with Lorentz-factor which is less sharp in case of CMB+EBL than for CMB only (see Fig. 2).

The photodisintegration of nuclei on CMB was only shortly mentioned by K. Greisen [28], and G.T. Zatsepin and V.A. Kuzmin [29], the first numerical calculations have been performed by F.W. Stecker [40] in 1969. Later Stecker and his collaborators developed this study of nuclei propagation through background radiation, providing the basic elements needed for calculations, namely, the nuclei photodisintegration and EBL models with its cosmological evolution [41]. Many practically important calculations of nuclei spectra have been performed by Allard, Olinto and Parizot, see review [36] for references.

Historically the GZK cutoff is related to production of pions on CMB $p + \gamma_{\text{cmb}} \rightarrow N + \pi$. To rename it including there also nuclei photodisintegration would be incorrect. Greisen, Zatsepin and Kuzmin just mentioned this process, considering it as nuclei interaction with CMB photons only. In this case beginning of the cutoff and its shape is completely different from the case of CMB+EBL, as one can see it from right panel of Fig.2. Authors of GZK cutoff explicitly emphasized connection of their work with CMB only. The extragalactic light was first considered in [39].

In contrast to GZK cutoff the nuclei photodisintegration cutoff has no well predicted observational signatures: in particular the energy position and shape of spectrum steepening are different for different nuclei.

3. Signatures of proton propagation through CMB.

Propagating through CMB, UHE protons undergo two interactions: photopion production $p + \gamma_{\text{cmb}} \rightarrow N + \pi$ and e^+e^- production $p + \gamma_{\text{cmb}} \rightarrow p + e^+ + e^-$. As a result, the proton spectrum is distorted: due to the first interaction it obtains a sharp steepening called *GZK cutoff* and due to the second one - shallow deepening, called *dip*. Both features depend not only on interactions but also on model-dependent quantities, e.g. on modes of propagation (diffusion or rectilinear propagation), on cosmological evolution of the sources, on source separation etc. These model-dependent distortions are especially strong for GZK feature.

The main strategy of this presentation as well as of works [42, 43, 44] is to distinguish the interaction signatures from the model-dependent ones.

This is possible to do using the *modification factor* $\eta(E)$ [45], some kind of theoretical spectrum, in which model-dependent features are suppressed or absent. For this aim we use the calculations which involve only one free physical parameter. One naturally expects that the calculated interaction signature in terms of modification factor cannot have the agreement with observations with good χ^2 , because the observational data include the model-dependent features described by many parameters, such as cosmological evolution of the sources, source separation etc. One free parameter is not enough to describe 4 - 5 different experiments with about 20 energy bins in each. As the next step we perform the *model-dependent* calculations which necessarily include many free parameters improving further the agreement. This analysis should be done in terms of natural spectrum, $J(E)$ or $E^3 J(E)$, where the model-dependent features are not suppressed.

However, the Nature has been more kind to us than we expected. The dip, in terms of modification factor with one free physical parameter (interaction-signature description) gave very good χ^2 agreement with observations of four experiments [46]: Yakutsk, AGASA, HiRes and Telescope Array (see section 3.1). The comparison with PAO data has a different story. Comparison in terms of modification factor with PAO observational data from ICRC 2007 (Merida) had good enough χ^2 (see [47]). However, as general prediction, the agreement must become worse with increasing statistics, and comparison of modification factor with PAO data 2010 has confirmed it. The reason is that for the difference in case of very small error bars the model-dependent effects are responsible. Indeed, as demonstrated in section 3.2 the 22% shift of PAO energy scale and cosmological evolution make the PAO spectrum in terms of $E^3 J(E)$ compatible with the pair-production dip with high accuracy. However, this interpretation contradicts the nuclei mass composition measured by PAO in energy region of the dip.

3.1. The dip in terms of modification factor

In this section the dip will be studied as a *signature* of UHE proton interaction with CMB, using the modification factor as a tool. The modification factor $\eta(E)$ is defined as the ratio of proton spectrum $J_p(E)$ calculated with all energy losses to the so-called unmodified spectrum $J_{\text{unm}}(E)$ in which only adiabatic energy losses (red-shift) are included:

$$\eta(E) = J_p(E)/J_{\text{unm}}(E). \quad (3)$$

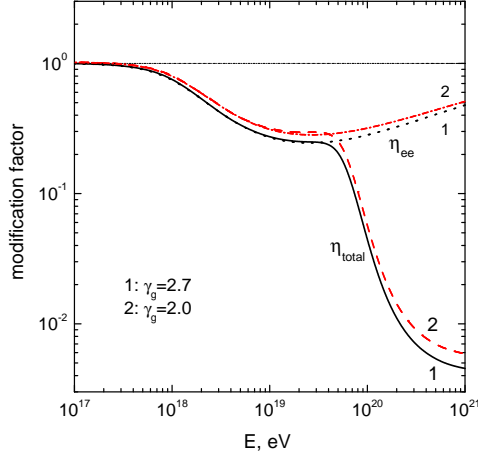


Figure 3: Modification factors for two generation indices $\gamma_g = 2.7$ and 2.0 . The dotted curve shows η_{ee} when only adiabatic and pair-production energy losses are included. The solid and dashed curves include also pion-production losses.

Modification factor is an excellent tool for *interaction signature*. As one might see the interactions enter only numerator and thus they are not suppressed in $\eta(E)$, while most other phenomena enter both numerator and denominator and thus they are suppressed or even cancelled in modification factor, the property being especially pronounced for the dip modification factor, which according to our calculations [44] depends very weakly on generation index γ_g and E_{\max} , on propagation mode, source separation within 1 - 50 Mpc, local source overdensity or deficit etc. The dip modification factor is modified strongly by presence of nuclei ($\gtrsim 15\%$). Modification factor for GZK feature is changing stronger.

Theoretical modification factors calculated for different source generation indices γ_g are presented in Fig. 3. If one includes in the calculation of $J_p(E)$ only adiabatic energy losses, then, according to its definition, $\eta(E) = 1$ (dash-dot line in Fig. 3). When e^+e^- -production is additionally included, one obtains spectrum $\eta(E)$ shown in Fig. 3 by the curves labeled as η_{ee} . With the pion photo-production process being also included, the GZK feature (curves “total”) appears. The observable part of the dip extends from the beginning of the GZK cutoff at $E \approx 40$ EeV down to $E \approx 1$ EeV, where $\eta \approx 1$. It has two flattenings: one at energy $E_a^{\text{tr}} \sim 10$ EeV and the other at $E_b \sim 1$ EeV. *The former automatically produces the ankle* (see Fig. 4)

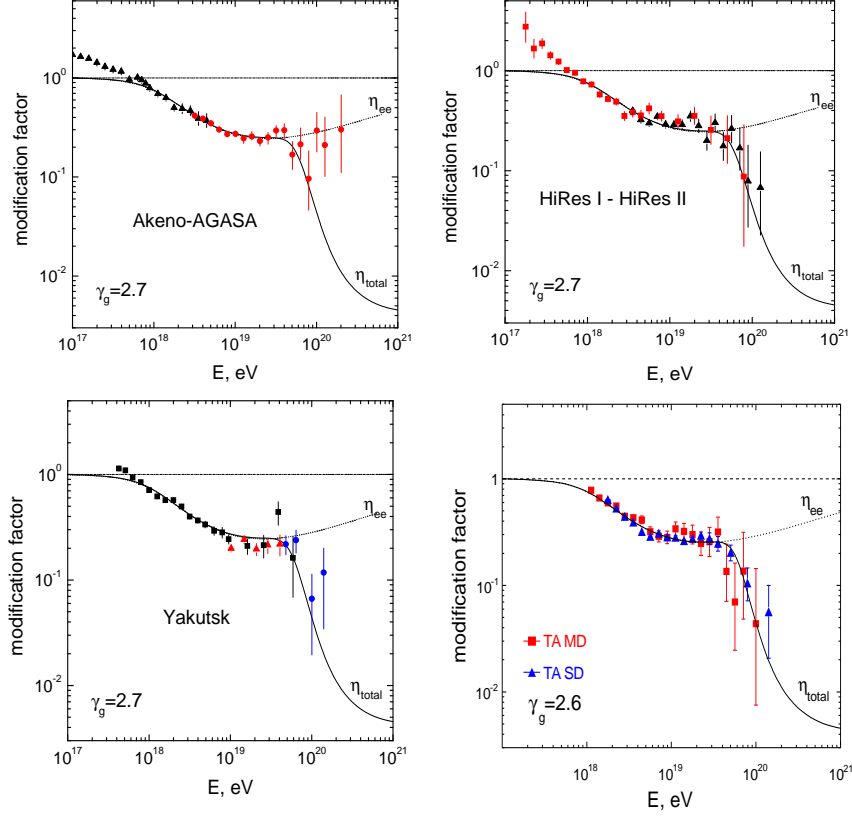


Figure 4: The predicted pair-production dip in comparison with Akeno-AGASA, HiRes, Yakutsk and Telescope Array data [46]. All these experiments confirm the dip behavior with good accuracy, including also the data of Fly’s Eye [46] (not presented here).

and the latter provides an intersection of the flat extragalactic spectrum at $E \leq 1$ EeV with the steeper Galactic one.

We discussed above the theoretical modification factor. The *observed* modification factor, according to definition, is given by the ratio of the observed flux $J_{\text{obs}}(E)$ and unmodified spectrum $J_{\text{unm}}(E) \propto E^{-\gamma_g}$, defined up to normalization as: $\eta_{\text{obs}} \propto J_{\text{obs}}(E)/E^{-\gamma_g}$. Here γ_g is the exponent of the generation spectrum $Q_{\text{gen}}(E_g) \propto E_g^{-\gamma_g}$ in terms of initial proton energies E_g . Fig. 4 shows that both the pair-production dip and the beginning of the GZK cutoff up to 80 EeV are well confirmed by experimental data [46] of Akeno-AGASA, HiRes, Yakutsk and Telescope Array (TA). The comparison of the theoretical dip with observational data includes only two free parameters:

exponent of the power-law generation spectrum γ_g (the best fit corresponds to $\gamma_g = 2.6 - 2.7$) and the normalization constant to fit the e^+e^- -production dip to the measured flux. The number of energy bins in the different experiments is 20 – 22. The fit is characterized by $\chi^2/\text{d.o.f.} = 1.0 - 1.2$ for AGASA, HiRes and Yakutsk data. This is a very good fit for *interaction signature* (see beginning of this section). For this fit we used the modification factor without cosmological evolution of sources. As was explained above, using a model approach with additional three parameters describing the cosmological evolution one can further improve the agreement.

In Fig. 4 one can see that at $E \lesssim 0.6$ EeV the experimental modification factor, as measured by Akeno and HiRes, exceeds the theoretical modification factor. Since by definition the modification factor must be less than one, this excess signals the appearance of a new component of cosmic rays at $E < E_{\text{tr}} \approx 0.6$ EeV, which can be nothing else but the Galactic cosmic rays. This interpretation is confirmed by transition of heavy component to the protons in the upper-left panel of Fig. 7, that with good accuracy occurs at the same energy. Thus, according to HiRes data the transition from extragalactic to Galactic cosmic rays, occurs at energy $E_{\text{tr}} \sim 0.6$ EeV and is accomplished at $E \sim E_b \approx 1$ EeV (see upper-left panel in Fig. 7 as example).

3.2. Pair-production dip as energy calibrator

The energy position of pair-production dip is rigidly fixed by interaction with CMB and thus it can serve as energy calibrator for the detectors.

As we already mentioned, it is difficult to expect that in terms of the modification factor the dip, described by one free physical parameter, can fit the observational data with minimum χ^2 . One can shift the observed energy bins by the recalibration factor λ_{cal} , within the systematic error of observations, to minimize χ^2 [43]. We shall refer to this procedure as ‘recalibration of energy scale’. We discuss first the dip in PAO spectrum [35] presented by the filled boxes in the left panel of Fig. 5. As it was already mentioned, because of very small statistical error bars it has too large χ^2 in comparison with pair-production dip terms of modification factor. We shall use then the model-dependent method in terms of $E^3 J(E)$ including the cosmological evolution $(1+z)^m$ up to z_{max} as shown in the left panel of Fig. 5. Using two more free parameters m and z_{max} we can reach better agreement with the modified shape of the dip shown by the solid curve in Fig. 5. Now we can shift the PAO energy bins by factor λ_{cal} reaching the minimum χ^2 . For

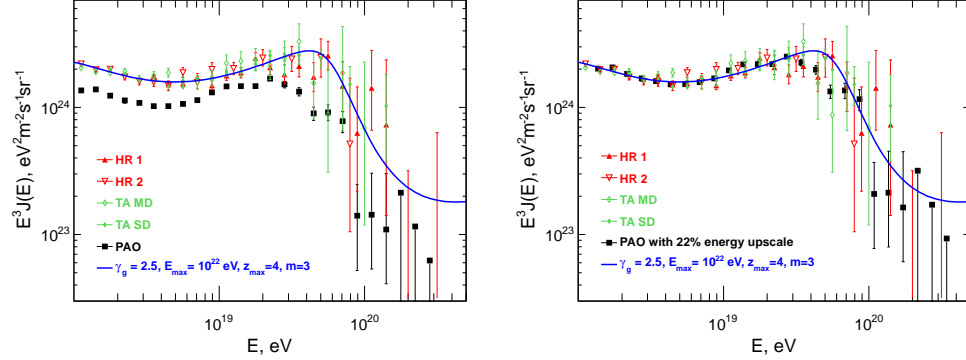


Figure 5: *Left panel:* Comparison of the PAO energy spectrum (filled boxes) with the HiRes and TA data fitted by theoretical pair-production dip (solid curve). *Right panel:* Spectra after energy recalibration of the PAO data with $\lambda_{\text{cal}} = 1.22$ (see the text).

this $\lambda_{\text{cal}} = 1.22$ is needed. As a result we obtain picture shown in the right panel of Fig. 5. We obtained not only the excellent agreement with the shape of the theoretical pair-production dip (solid curve) but also the good agreement with absolute fluxes of HiRes and TA. Note that disagreement with GZK cutoff remains for the three energy bins in energy interval 35 – 52 EeV. Recalibration with help of pair-production dip for all five detectors (HiRes, Telescope Array, PAO, AGASA and Yakutsk) is shown in Fig. 6. Recalibration factor $\lambda_{\text{cal}} = 1$ for HiRes/TA is based on the scale factor which correctly describes the pair-production dip and GZK cutoff in differential and integral ($E_{1/2}$) spectra.

3.3. GZK cutoff in HiRes and Telescope Array data

The two largest Extensive Air Shower (EAS) detectors, HiRes [30] and Pierre Auger Observatory [32] have observed a sharp steepening in the UHECR spectrum at $E \gtrsim (30 - 50)$ EeV. Both collaborations claimed that the observed steepening is consistent with the GZK cutoff. But as a matter of fact, there is a dramatic conflict between these two results, which still leaves the problem open. In this subsection we analyze data of the HiRes which provide a strong evidence in favour of the GZK cutoff. These data are supported also by the TA data [31]. The data of PAO will be considered in the next subsection.

To interpret convincingly the spectrum steepening as the GZK cutoff one must prove that (*i*) energy scale of the cutoff and its shape correspond to

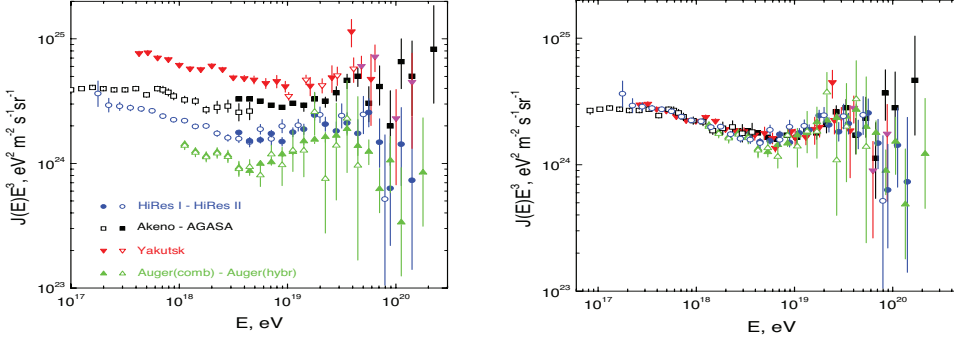


Figure 6: *Left panel:* Original fluxes from all detectors (fluxes from HiRes and TA are approximately the same). *Right panel:* Spectra after energy recalibration by pair-production dip: $\lambda_{\text{cal}} = 1$ for HiRes/TA, $\lambda_{\text{cal}} = 1.22$ for PAO, $\lambda_{\text{cal}} = 0.75$ for AGASA and $\lambda_{\text{cal}} = 0.625$ for Yakutsk.

theoretical predictions and (ii) the measured mass composition is strongly dominated by protons. In HiRes the mass composition is determined from $\langle X_{\text{max}} \rangle(E)$, average depth of atmosphere in g/cm^2 , where a shower with energy E reaches maximum, and $\text{RMS}(X_{\text{max}})$, which is the width of the distribution over X_{max} . These values measured by HiRes are displayed in Fig. 7. From the left-upper panel of Fig. 7 one can see that the chemical composition changes from very heavy elements, probably Iron, at $E \sim 0.1$ EeV, (data of HiRes-MIA [48]) to protons at $E \sim 1$ EeV (data of HiRes [22]). $\text{RMS}(X_{\text{max}})$, a very sensitive tool for mass composition, also provides evidence for a proton-dominated composition at $E \gtrsim 1$ EeV and up to the highest energies (see upper-right panel of Fig. 7). Differential energy spectrum of the GZK feature in the form of modification factor (left-lower panel) is in a reasonably good agreement with the theoretical prediction, though better statistics at higher energies is still needed for a final conclusion.

The *integral energy spectrum* of UHE protons, $J_p(> E)$, has another specific characteristic of the GZK cutoff, the energy $E_{1/2}$ [45]. It is based on the observation that the calculated integral spectrum below 50 EeV is well approximated by a power-law function: $J_p(> E) \propto E^{-\tilde{\gamma}}$. At high energy this spectrum is steepening due to the GZK effect. The energy where this steep part of the spectrum equals to the half of its power-law extrapolation, $J_p(> E) = KE^{-\tilde{\gamma}}$, defines the value of $E_{1/2}$. This quantity is found to be practically model-independent; it equals to $E_{1/2} = 10^{19.72} \text{eV} \approx 52.5$ EeV [45].

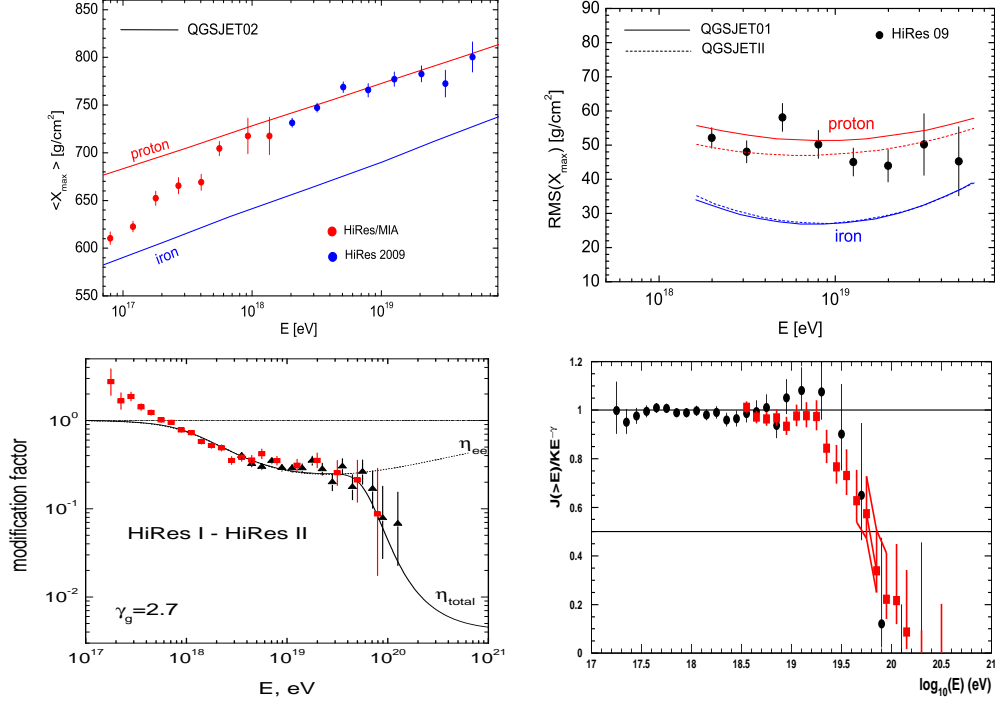


Figure 7: Mass composition and GZK cutoff as measured by the HiRes detector. In two upper panels $\langle X_{\max} \rangle$ (left) and RMS (right) are presented as function of the energy. Both agree with a pure proton composition, shown by curves labeled 'proton'. The left-lower panel shows differential energy spectrum in terms of the modification factor. One can see a good agreement with the predicted shape of the GZK cutoff. The right-lower panel shows the quantity $E_{1/2}$ in the integral spectrum. This energy, a characteristic of the GZK cutoff, is found as $E_{1/2} = 10^{19.73 \pm 0.07}$ eV in good agreement with theoretical prediction $E_{1/2} = 10^{19.72}$ eV (see the text).

Fig. 7 demonstrates how the HiRes collaboration found $E_{1/2}$ from observational data [49]. The ratio of the measured integral spectrum $J(>E)$ and the low-energy power-law approximation $KE^{-\tilde{\gamma}}$ was plotted as a function of energy. This ratio is practically constant in the energy interval 0.3 – 40 EeV, indicating that the power-law approximation is a good fit, indeed. At higher energy the ratio falls down and intersects the horizontal line 0.5 at the energy defined as $E_{1/2}$. It results in $E_{1/2} = 10^{19.73 \pm 0.07}$ eV, in an excellent agreement with the predicted value.

Thus, one may conclude that the HiRes data presented in Fig. 7 indicate the proton-dominated chemical composition and the presence of the GZK

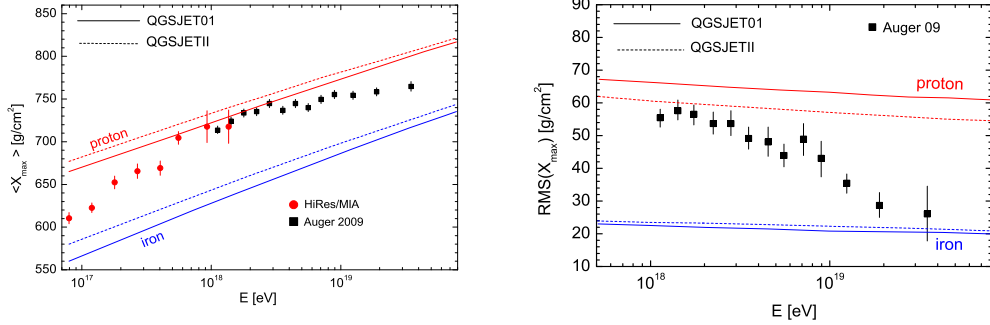


Figure 8: *Left panel:* Auger data [50] for $\langle X_{\max} \rangle$ as function of the energy (left panel) and for $\text{RMS}(X_{\max})$, the width of the distribution over X_{\max} , (right panel). The calculated values for protons and Iron are given according to QGSJET01 [51] and QGSJET II [52] models. One can see from the right panel that RMS distribution becomes more narrow with increasing energy which implies a progressively heavier mass composition.

cutoff in both differential and integral spectra. The conclusion about proton composition is further supported by the recent TA data [31].

3.4. PAO data: energy spectrum and mass composition

In subsection 3.2 we demonstrated that the dip shape, as observed by PAO, can agree after recalibration with energy spectra of HiRes/TA and other detectors (see Figs. 5 and 6). The agreement of the PAO and HiRes/TA spectra is related to low energy part of the energy spectrum in the right panel of Fig. 5. At higher energies statistical uncertainties are too large to distinguish between the spectra.

While the HiRes and TA spectra are compatible with the GZK cutoff, the Auger spectrum is not. The steepening in the PAO spectrum starts at energy $E = 25.7 \pm 1.2$ EeV [25, 35], lower than $E_{\text{GZK}} \simeq 50$ EeV, and in three successive energy bins in the interval 35 – 52 EeV the PAO flux is significantly lower than one predicted for the GZK shape as shown in the right panel of Fig. 5. We could not reconcile the PAO cutoff shape with the GZK behavior by including in the calculations different generation indices γ_g , evolution regimes, low acceleration maximum energy E_{\max} , local overdensity of sources etc.

This disagreement is quite natural for the PAO mass composition which, in contrast to HiRes and TA, show strong dominance of nuclei (see Fig. 8). A steepening in the end of the of the nuclei spectrum, as calculations show,

is quite different from that of protons (GZK cutoff). The most reliable data on mass composition are given by elongation curve $X_{\max}(E)$ and especially by $\text{RMS}(X_{\max}(E))$. In the Auger data the latter steadily decreases with energy and approaches the Iron value at $E \approx 35$ EeV. Low RMS, i.e. small fluctuations, is a typical and reliable feature of the heavy nuclei composition. These data are further strengthened by other PAO measurements provided by surface detectors. They allow to extract two other mass-composition dependent quantities: the atmospheric depth $\langle X_{\max}^{\mu} \rangle$, where muon-production rate reaches maximum, and maximum zenith angle ϑ_{\max} determined by the signal rise-time in surface Cerenkov detectors. Measurements of both quantities, [53] and [54], confirm the heavy mass composition and its dependence on energy obtained with the help of $\langle X_{\max} \rangle(E)$ and $\text{RMS}(X_{\max})$,

Our further analysis of the Auger spectrum and mass composition is based on the following two observations:

(i) According to the HiRes (Fig. 7) and PAO (Fig. 8) data, the observed primaries at energy (1 – 3) EeV are predominantly protons or nuclei not heavier than Helium.

These particles cannot be galactic, otherwise, as MC simulations [55] show, galactic anisotropy would be too large.

(ii) The particles at higher energies are extragalactic nuclei with the charge number Z increasing with energy.

This observation is naturally explained by rigidity dependent acceleration in the sources $E_i^{\max} = Z_i \times E_p^{\max}$, since at each energy $E = ZE_p^{\max}$ the contribution of nuclei with smaller $Z' < Z$ vanishes. It was demonstrated in [56] that to avoid a proton dominance at the highest energies, one must assume that the maximum energy of the accelerated protons is limited, $E_p^{\max} \lesssim (4 - 10)$ EeV and thus $E_{\text{Fe}}^{\max} \sim 200$ EeV. The calculated spectrum [56] explains well the PAO energy spectrum, however a problem remains to explain simultaneously energy spectrum and mass composition. Somewhat similar calculations are performed in [57] (see Fig. 4 there), and [58].

4. Status of ankle as transition from galactic to extragalactic cosmic rays.

As was discussed in section 1 there are two features in the observed CR spectrum, where transition from galactic to extragalactic cosmic rays is expected: the second knee and ankle.

The *second knee* at energy $E_{\text{scn}} \approx (0.4 - 0.7)$ EeV as transition feature corresponds well to the Standard Model (SM) of Galactic CRs, where maximum energy of acceleration corresponds to Iron knee, $E_{\text{max}} \approx (0.08 - 0.1)$ EeV.

The *ankle* is located at $E_a \approx (4 - 5)$ EeV according to all data, and as a feature of transition it needs another high-energy galactic component beyond SM. On the other hand the ankle appears automatically as the *dip feature* in Akeno-AGASA, HiRes, Yakutsk and TA data (see Fig. 4) and also in Auger data (Fig.5 right panel) after recalibration of energies with $\lambda = 1.22$ and inclusion of evolution of the sources in theoretical prediction. At this comparison the power-law spectra approximation is not needed. Note that ankle in this case is a feature produced by interaction of extragalactic protons with CMB. We will demonstrate below that interpretation of the ankle as transition feature contradicts the observational data of the Auger, HiRes and TA detectors.

The key data used in a proof is given by energy interval (1 - 3) EeV where the observed mass composition in HiRes, TA and Auger agrees with pure proton composition and cannot be heavier than Helium (for Auger data see Fig. 8). In the ankle model of transition this interval is below the ankle at $E_a \approx (4 - 5)$ EeV and thus must have galactic origin. Meanwhile, the Monte-Carlo simulations (see e.g. [59]) and most convincingly the recent one [55], show that predicted anisotropy exclude the galactic protons and light nuclei at $E \gtrsim 1$ EeV as observed primary particles. This conclusion is further strengthened by recent upper limit on the anisotropy observed by the Auger collaboration [60].

In fact, the conclusion about ruling out the ankle as transition feature has been already made in [61] and more recently in [62] from analysis of elongation curve $X_{\text{max}}(E)$. One can see from right-upper and right-lower panels of Fig. 10 in [62], the strong contradiction of the ankle model with the $X_{\text{max}}(E)$ data of Auger and HiRes in (1 - 5) EeV energy interval.

The analysis above proves that transition from galactic to extragalactic CRs occurs below 1 EeV, where the only visible spectral feature is the second knee. Together with the proton mass composition at (1 - 3) EeV observed in HiRes, TA and Auger experiments it gives one more support to the pair-production nature of the observed dip and the dip model developed in [42, 43, 44].

An alternative explanation of the ankle observed in PAO at $E_a \approx 4$ EeV is given by transition at this energy from extragalactic protons to extragalactic nuclei. However according to PAO observations [50] the energy of this tran-

sition using the change in elongation rate and in $\text{RMS}(E)$ is given by $E_{\text{tr}} = 2.40^{+0.42}_{-0.72}$ EeV to be compared with position of ankle $E_a = (4.17 \pm 0.1)$ EeV. If to assume $E_{\text{tr}} \approx E_a$ the Auger spectrum and mass composition can be explained by disappointing model [56]. The transition from galactic CRs (Iron) to extragalactic protons occurs at the second knee. Transition from extragalactic protons to extragalactic nuclei occurs near the maximum of acceleration energy for protons $E_p^{\text{max}} \approx 4$ EeV. This energy provides transition from protons to heavier nuclei because their maximum energy $E_A^{\text{max}} = ZE_p^{\text{max}}$ is higher. The observed highest energy steepening can be explained as nuclei-photodisintegration cutoff.

5. Conclusions.

The most important result of analysis performed in this paper is the conclusion on interpretation of *ankle*, observed at $E_a \sim 4$ EeV in all experiments. This feature is usually interpreted as transition from galactic to extragalactic CRs. The presented analysis is based on consensus about mass composition measured by HiRes, TA and Auger detectors, which show that at energies (1 - 3) EeV (i.e. below the ankle) the primaries are protons or nuclei not heavier than Helium. Having galactic origin, these particles must show the big anisotropy [55] in contrast to low anisotropy measured recently [60] by Auger detector. In fact this analysis only enhances the similar conclusion reached in papers [61] and [62] about ruling out the models with transition at the ankle. using the measured elongation curves $X_{\text{max}}(E)$.

In the light of these results, the transition must occur at lower energies, most probably at the *second knee* from Iron galactic component to proton extragalactic component as the *dip* model predicts [42, 43, 44]. It strengthens further the dip model.

The dip model is based on the dip as a signature of e^+e^- pair-production in interaction of UHE protons with CMB: $p + \gamma_{\text{cmb}} \rightarrow p + e^- + e^+$. The characteristic which is sensitive mostly to interaction is given by *modification factor* $\eta(E) = J_p(E)/J_{\text{unm}}(E)$, where unmodified proton flux $J_{\text{unm}}(E)$ is calculated only with adiabatic energy losses taken into account, while $J_p(E)$ is calculated accounting for all energy losses. One may see that interactions enter only numerator and thus modification factor is very sensitive to interactions, while most other phenomena enter both, numerator and denominator, and thus they are suppressed or even cancelled in modification factor. The theoretical modification factor is presented in Fig. 3 and one can see that it

practically does not depend on the generation index γ_g . Another property of modification factor is $\eta(E) \rightarrow 1$ at $E \rightarrow 1$ EeV. Comparing the theoretical and experimental modification factors (see Fig. 4) one can use only one free physical parameter for description about 25 bins in each of four experiments, however agreement is quite good. It confirms that observed dip is really produced by $p + \gamma_{\text{cmb}} \rightarrow p + e^- + e^+$.

One naturally expects that the calculated interaction signature in terms of modification factor cannot have the agreement with high-statistics observations with very good χ^2 , because the observational data include the model-dependent features described by many parameters, such as cosmological evolution of the sources, source separation etc. When statistics increases, agreement with modification factor must become worse as it happened with Auger data. As the next step we performed the *model-dependent* calculations which necessarily include many free parameters describing all important physical effects. This analysis should be done in terms of natural $E^3 J(E)$ spectrum, where the model-dependent features are not suppressed.

The dip has the fixed energy position and shape, therefore it can serve as natural energy calibrator. Shifting the energy scale in each four experiments by factor λ , i.e. shifting each energy bin in each experiment a by factor λ_a , one can reach χ^2_{min} for each experiment. Interestingly enough that as a result of this procedure the Auger data show the dip (see right panel of Fig. 5) and fluxes of all experiments coincide, as one can see in Fig. 6 and in Fig. 11 of Ref. [43]. We assume there $\lambda = 1$ for HiRes experiment, because it has the correct scales in the form of beginning of GZK cutoff and $E_{1/2}$.

The dip is valid for proton-dominated spectrum. Mixing of protons with 15% of nuclei modifies the dip shape.

The different mass composition presented as a result of direct measurements in the HiRes and TA experiments, on one side, and in Auger experiments, on the other side, is at present the main conflict in UHECR. While the data of HiRes/TA show the proton-dominated mass composition at all energies above 1 EeV, a few different methods of mass-composition measurement in Auger experiments demonstrate the nuclei-dominated composition starting from energy $E \sim 4$ EeV and being steadily heavier as energy increases. Data of all three experiments, HiRes, TA and Auger, coincide in narrow energy interval (1 - 3) EeV, where composition is proton-dominated. Each of two possibilities can be viable within two contradicting models.

The model for description of HiRes and TA data is a proton-dominated one with transition from galactic (Iron nuclei) to extragalactic (proton) com-

ponent at the second knee. The presence of two features, the pair-production dip and GZK cutoff, are compulsory for such mass compositions, and these features are observed indeed as the shape of the dip and beginning of the GZK cutoff, together with value of $E_{1/2}$. The dip model describes all these features numerically.

The Auger mass composition implies quite different scenario. The transition from galactic to extragalactic CRs occurs at the second knee ($E_{\text{skn}} \approx (0.4 - 0.7)$ EeV) as the only visible spectral feature between the Iron knee (galactic feature) and the ankle (extragalactic feature). The ankle at $E_a \sim 4$ EeV may be produced by transition from extragalactic proton component at $E < 4$ EeV to extragalactic heavy nuclei component, though according to Auger data [50] this transition occurs at lower energy $E \approx 2.4$ EeV. Proton component disappears because of low $E_p^{\text{max}} \sim 4$ EeV at acceleration [56], and heavier nuclei progressively dominate at higher energies because of the higher acceleration energies $E_A^{\text{max}} = ZE_p^{\text{max}}$, or because of diffusion, or both. The highest-energy spectrum suppression, observed by Auger at $E_{\text{supp}} = 25.7 \pm 1.2$ EeV [35] is too low for GZK cutoff. It can be explained as nuclei-photodisintegration cutoff.

The Auger scenario is characterised by very specific behaviour of $X_{\text{max}}(E)$ and RMS(E) curves since protons appear in a relatively small energy range (1 - 3) EeV. In this range X_{max} and RMS reach the highest values, typical for protons, with lower values starting at both ends of these interval, because of transition to galactic Iron (lower end) and extragalactic nuclei (upper end). Intersection of galactic spectrum (Iron) with extragalactic protons corresponds to maximum of RMS.

All three biggest experiments use the fluorescent detectors as the main tool of measurements. The contradicting results are connected with some difference in the data analysis. Close collaboration between Telescope Array and Auger teams may resolve this problem in the nearest future. The role of new experiments is less significant: already now there two experiments which confirm proton-dominated composition and one - nuclei-dominated composition. Science is a choice, but not elections.

Acknowledgment

This paper is based on the joint works and many discussions with my co-authors Roberto Aloisio, Askhat Gazizov and Svetlana Grigorieva. I am mostly grateful to them for efficient and pleasant collaboration. The work was

partly supported by Ministry of Science and Education of Russian Federation (agreement 8525).

References

- [1] V.L. Ginzburg, Soviet Physics Uspekhi, **51** (1953), 343,
- [2] V.L. Ginzburg and S.I. Syrovatskii, Soviet Physics Uspekhi, **71** (1960) 411.
- [3] T. Gold and F. Hoyle, Proc. of Paris Symposium on Radio Astronomy (Stanford Univ. Press), (1959), 104.
- [4] G.R. Burbidge, Progress Theor. Phys. **27** (1962) 999.
- [5] G.R. Burbidge and F.Hoyle Proc. Phys. Soc. **84** (1964) 141.
- [6] V.L. Ginzburg and S.I. Syrovatskii, The Origin of Cosmic Rays, (Pergamon Press, Oxford, 1964), Russian original 1963.
- [7] A.M. Hillas, Ann. Rev. Astron. Astrophys. **22** (1984) 425.
- [8] P. Streekumar et al., Phys. Rev. Lett., **70** (1993) 127.
- [9] A.A. Abdo et al., arXiv: 1008.2127.
- [10] S.I. Syrovatskii, Soviet Astronomy **3** (1959) 22.
- [11] G. F. Krymsky, Sov. Phys. Dokl. Acad. Nauk USSR **243** (1977) 1306;
W. I. Axford et al. Proc. 15th ICRC, Plovdiv **11**, (1977) 132;
A. R. Bell, Mon. Not. RAS **182**, (1978) 147 ;
R. D. Blandford, and J. P. Ostriker, Astrophys. J. **221**, (1978) L229.
- [12] P.O. Laggage and C.J. Cesarsky, Astron. Astrophys **125** (1983) 249.
- [13] A. R. Bell, and S. G. Lucek, MNRAS **321** (2001) 433.
- [14] G. Kulikov, and G. Khristiansen, JETP **35** (1958) 635.
- [15] W.D. Apel et al. [KASCADE-Grande Collab.], Phys. Rev. Lett. **107** (2011) 171104, arXiv:1107.5885

- [16] M. Nagano et al. [Akeno Collab.], J. Phys. G: Nucl. Part. Phys. **18**, (1992) 423;
D. J. Bird et al. [Fly’s Eye Collab.], Phys. Rev. Lett. **71**, (1993) 3401 ;
A. V. Glushkov et al. [Yakutsk Collab.], JETP Lett. **73**, (2001) 115
- [17] D. R. Bergman, and J. W. Beltz, J. Phys. G **34**, (2007) 359, arXiv:0704.3721
- [18] J. Linsley, Proc. 8th ICRC (Jaipur 1963) **4**, (1963) 77.
- [19] J. Linsley, Phys. Rev. Lett. **10**, (1963) 146.
- [20] J. Linsley, Scientific American **239**, (1978).
- [21] T.K. Gaisser, arXiv:1010.5996.
- [22] P. Sokolsky for HiRes Collaboration, Nucl. Phys. B (Proc. Suppl.) **196**, (2009) 67 and P. Sokolsky for HiRes Collaboration “Final Results from the HiRes experiment” ISVHECR, Batavia IL, USA (2010)
- [23] T. Abu-Zayyad et al (Telescope Array Collaboration) arXiv:1205.5067.
- [24] The Pierre Auger Collaboration, Phys. Lett. B **685**, (2010) 239.
- [25] K-H Kampert for the Pierre Auger Collaboration, arXiv:1207.4823
- [26] S.D. Wick, C.D. Dermer, A. Atoyan, Astropart. Phys. **21**, (2004) 125.
- [27] A. Galvez, A. Kusenko, S. Nagataki, Phys. Rev. Lett. **105**, (2010).
- [28] K. Greisen, Phys. Rev. Lett. **16**, 748 (1966)
- [29] G. T. Zatsepin, and V. A. Kuzmin, Pisma Zh. Experm. Theor. Phys. **4**, 114 (1966)
- [30] R. U. Abbasi et al. Phys. Rev. Lett. **100**, (2008) 101101.
- [31] C. C. H. Jui [Telescope Array Collab.], arXiv:1110.0133;
Y. Tsunesada [Telescope Array Collab.], arXiv:1111.2507
- [32] J. Abraham et al., Phys. Rev. Lett. **101**, 06110.1 (2008)
- [33] R. Aloisio, V. Berezhinsky, S. Grigorieva I, Astropart. Phys. **41** (2013) 73.

- [34] R. Aloisio, V. Berezhinsky, S. Grigorieva I, *Astropart. Phys.* **41** (2013) 94.
- [35] F. Salamida (for the Pierre Auger Collaboration) ICRC2011 arXiv:1107.4809.
- [36] D. Allard, *Astropart. Phys.* 39-40 (2012) 33.
- [37] V.S. Berezhinsky and G.T. Zatsepin, *Soviet Journal of Nuclear Physics*, **13** (1971) 453.
- [38] V.S. Berezhinsky, S.I. Grigorieva, G.T. Zatsepin, *Proc. of 14th Int. Cosmic Ray Conf, (Munich)* **2** (1975), 711.
- [39] N.M. Gerasimova and I.L. Rosental, *JETP*, **41** (1961) 488.
- [40] F.W. Stecker, *Phys. Rev.* **180** (1969) 1264.
- [41] J.L. Puget and F.W. Stecker, *Proc. of 14th Int. Cosmic Ray Conf, (Munich)* **2** (1975), 734; J.L. Puget, F.W. Stecker, J.H. Bredekamp, *Ap.J.*, **205** (1976) 638; M.A. Malkan, F.W. Stecker, *Ap.J.* **496** (1998) 13; M.A. Malkan, F.W. Stecker, *Ap.J.* **555** (2001) 641, F.W. Stecker, M.H. Salamon, *Ap. J.* **512** (1999) 521, F.W. Stecker, M.A. Malkan, S.T. Scully, *Ap.J.* **648** (2006) 774.
- [42] V. Berezhinsky, A. Z. Gazizov, and S. I. Grigorieva, *Phys. Lett. B* **612**, 147 (2005); astro-ph/0502550
- [43] V. Berezhinsky, A. Z. Gazizov, and S. I. Grigorieva, *Phys. Rev. D* **74**, 043005 (2006); hep-ph/0204357
- [44] R. Aloisio, V. Berezhinsky, P. Blasi, A. Gazizov, S. Grigorieva, and B. Hnatyk, *Astropart. Phys.* **27**, 76 (2007); astro-ph/0608219
- [45] V. S. Berezhinsky, and S. I. Grigorieva, *Astron. Astrophys.* **199**, 1 (1988)
- [46] V. P. Egorov et al. [Yakutsk Collab.], *Nucl. Phys. B (Proc. Suppl.)* **3**, 136 (2004);
K. Shinozaki et al. [AGASA Collab.], *Nucl. Phys. B (Proc. Suppl.)* **3**, 151 (2006);
R. U. Abbasi et al. [HiRes Collab.], *Phys. Rev. Lett.* **92**, 151101 (2004);
C. C. H. Jui [Telescope Array Collab.], arXiv:1110.0133
D. J. Bird et al. [Fly’s Eye Collab.], *Astrophys. J.* **424**, 491 (1994).

- [47] V. Berezhinsky, Journal of Physics: Conference Series (TAUP 2007, eds. K. Inoue, A. Suzuki, T. Mitsui) **120**, 012001 (2008)
- [48] R. U. Abbasi et al. [HiRes-MIA Collab.], Phys. Lett. B **556**, 1 (2003)
- [49] R. U. Abbasi et al. [HiRes Collab.], arXiv:astro-ph/0703099v1
- [50] P.P. San Luis for the Pierre Auger Collaboration, 32nd Int. Cosmic Ray Conference, Beijing 2011, 1107.4804
- [51] N. N. Kalmykov, and S. S. Ostapchenko, A. I. Pavlov, Bull. Russ. Acad. Sci. Phys. **58**, 1966 (1994); Nucl. Phys. Proc. Suppl. **52B**, 17 (1997)
- [52] S. Ostapchenko, Phys. Rev. D **83**, 014018 (2011); Phys. Rev. D **74**, 014026 (2006); Nucl. Phys. Proc. Suppl. **151 B**, 143 (2006)
- [53] D. Garcia-Gamez, for the Pierre Auger Collaboration, arXiv:astro-ph/1107.4804
- [54] L. Gazon, for the Pierre Auger Collaboration, arXiv:astro-ph/1201.6265
- [55] G. Giacinti, M. Kachelrieß, D. V. Semikoz, G. Sigl, JCAP **1207**, 031 (2012), arXiv:1112.5599
- [56] R. Aloisio, V. Berezhinsky, A. Gazizov, Astropart. Phys. **34**, 620 (2011); J. Phys. Conf. Ser. **337**, 012042 (2012)
- [57] D. Allard arXiv:1111.3290
- [58] A. M. Taylor, M. Ahlers, F. A. Aharonian, Phys. Rev. D **84**, 105007 (2011), arXiv: 1107.2055
- [59] V. Berezhinsky, S. Grigorieva, M. Marchesini, Proc. 9th Int. Workshop, “Neutrino Telescopes”, p.13, 2011, ed. Milla Baldo-Ceolin, Venice, March 6 - 9, 2011.
- [60] P. Abreu et al. , The Pierre Auger Collaboration, arXiv:1212.3083.
- [61] R. Aloisio, V. Berezhinsky, P. Blasi, S. Ostapchenko, Phys. Rev. D **77**, 025007 (2008).
- [62] R. Aloisio, V. Berezhinsky, A. Gazizov, Astrop. Phys. **39-40** (2012) 129.